Supplementary Materials for

Freeform Cell-Laden Cryobioprinting for Shelf-Ready Tissue Fabrication and Storage

Hossein Ravanbakhsh, Zeyu Luo, Xiang Zhang, Sushila Maharjan, Hengameh Sadat Mirkarimi, Guosheng Tang, Carolina Chávez-Madero, Luc Mongeau, Yu Shrike Zhang*

*Corresponding author. Email: yszhang@research.bwh.harvard.edu

This PDF file includes:

Figures S1 to S20
Tables S1 to S3

Other Supplementary Materials for this manuscript include the following:
Movies S1 to S9

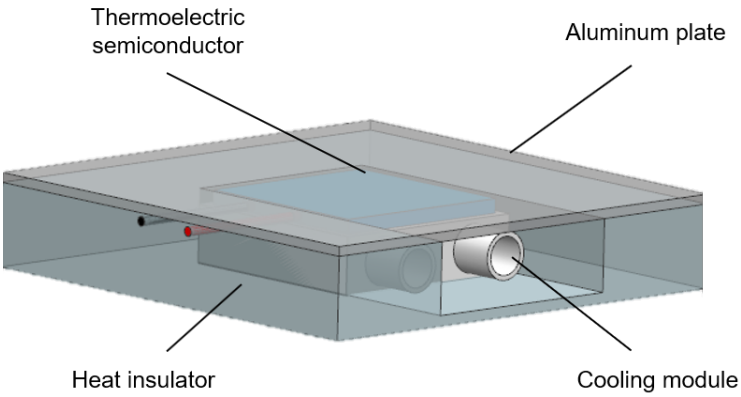

Figure S1.

Schematic of the freezing plate used as the substrate for cryobioprinting. The freezing plate was cooled using a pair of semiconductors, which were powered by a DC voltage-generator. The surface temperature could be adjusted by changing the output voltage on the DC power. The semiconductors were cooled down *via* a water-based cooling module.

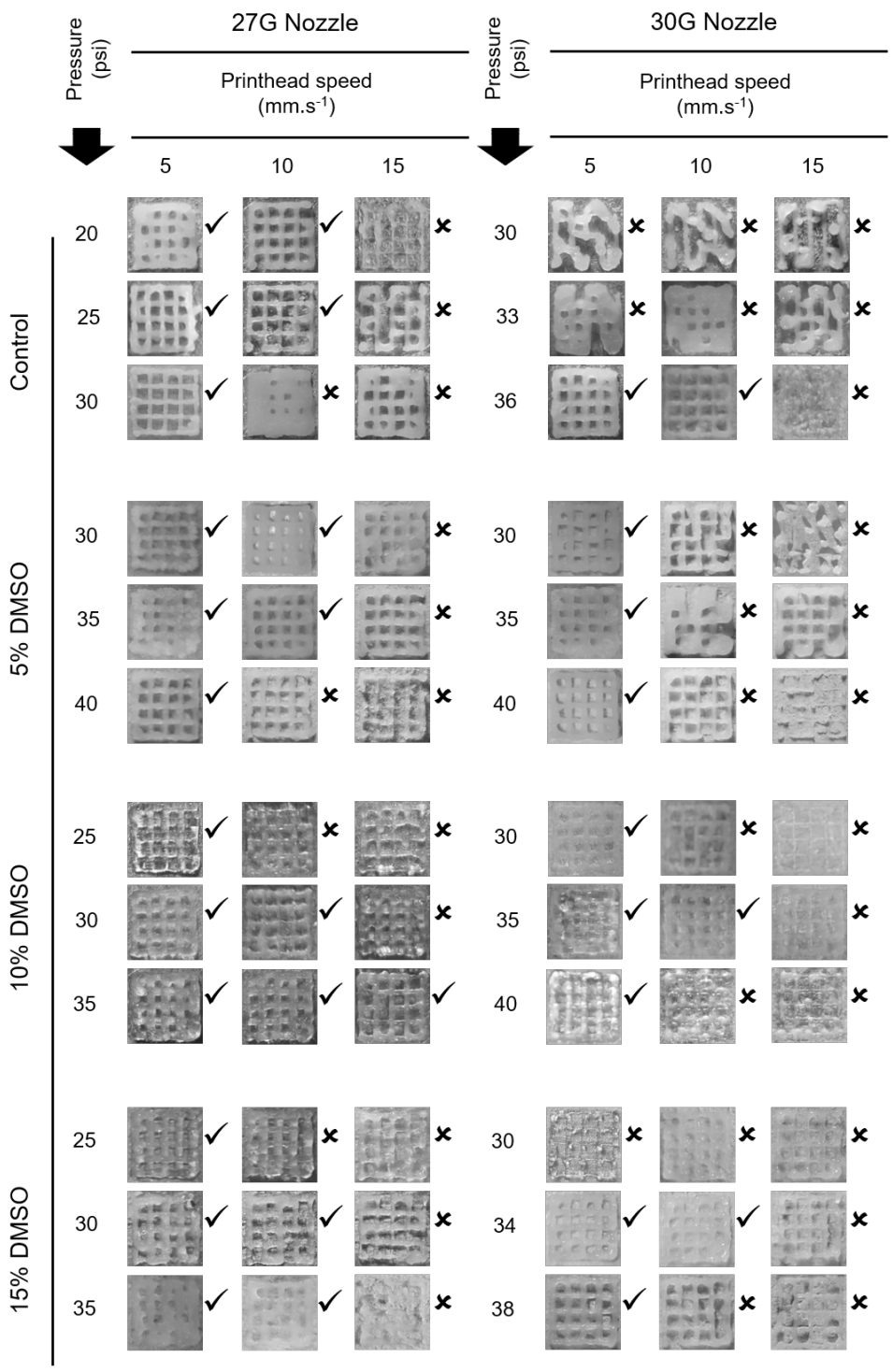

Figure S2.

Effects of nozzle size, pressure, printhead moving speed, and DMSO concentration on the printability of the cryoprotective GelMA bioink by comparing cryobioprinted 8×8-mm² grids. The checkmarks were used to denote the high-fidelity samples with structural integrity over 90% of the printed grids, *i.e.*, acceptable samples, while the cross signs represent

poor/unsuccessful cryobioprinting jobs. The addition of DMSO as the CPA had negligible effects on the printability of GelMA.

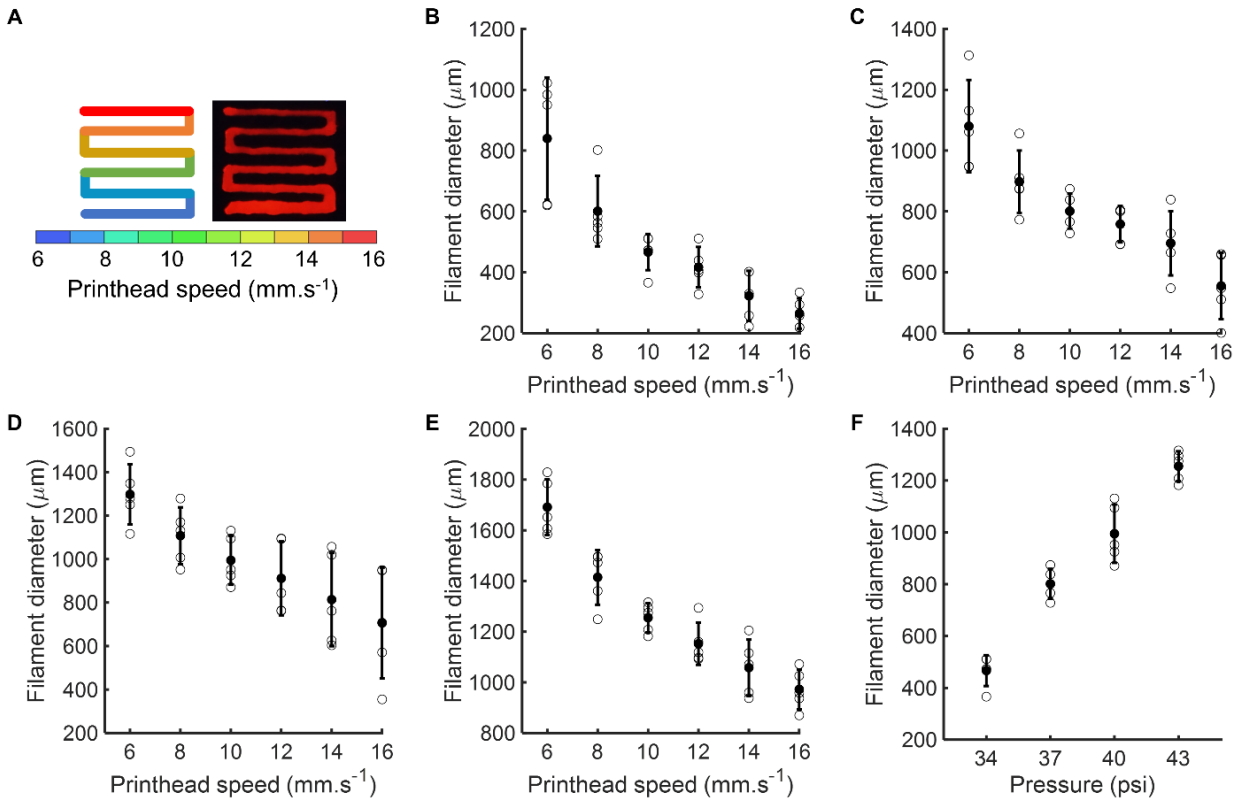

Figure S3.

Effects of printhead moving speed and pressure on filament diameter. (**A**), Bioprinting of a continuous filament using a 27G nozzle with different moving speeds for parametrically studying the effect of pressure (P) and speed (V) on the filament diameter. (**B**), P=34 psi. (**C**), P=37 psi. (**D**), P=40 psi. (**E**), P=43 psi. (**F**), V=10 mm.s^{-1}. n = 5.

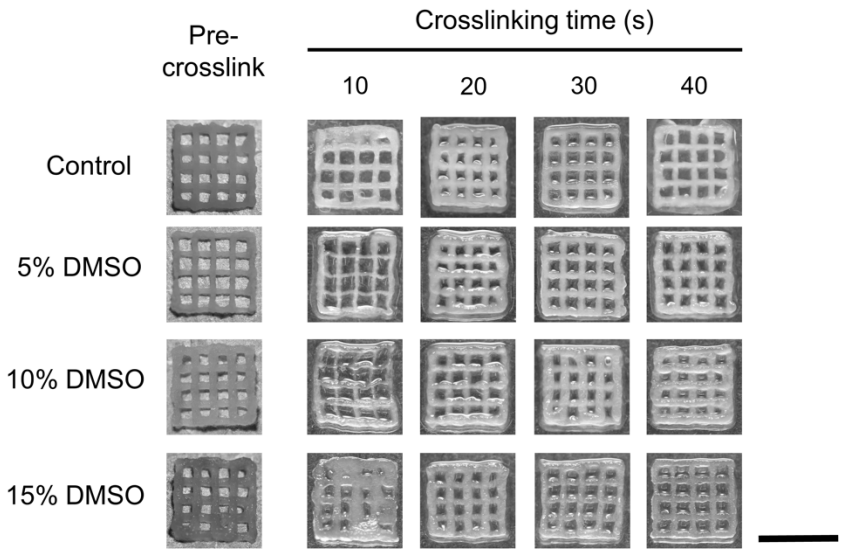

Figure S4.

The effect of UV exposure time on the fidelity of the cryobioprinted grid structures. The samples with 10 s of UV crosslinking were not fully crosslinked as the exposure time was not adequate. Scale bar: 8 mm.

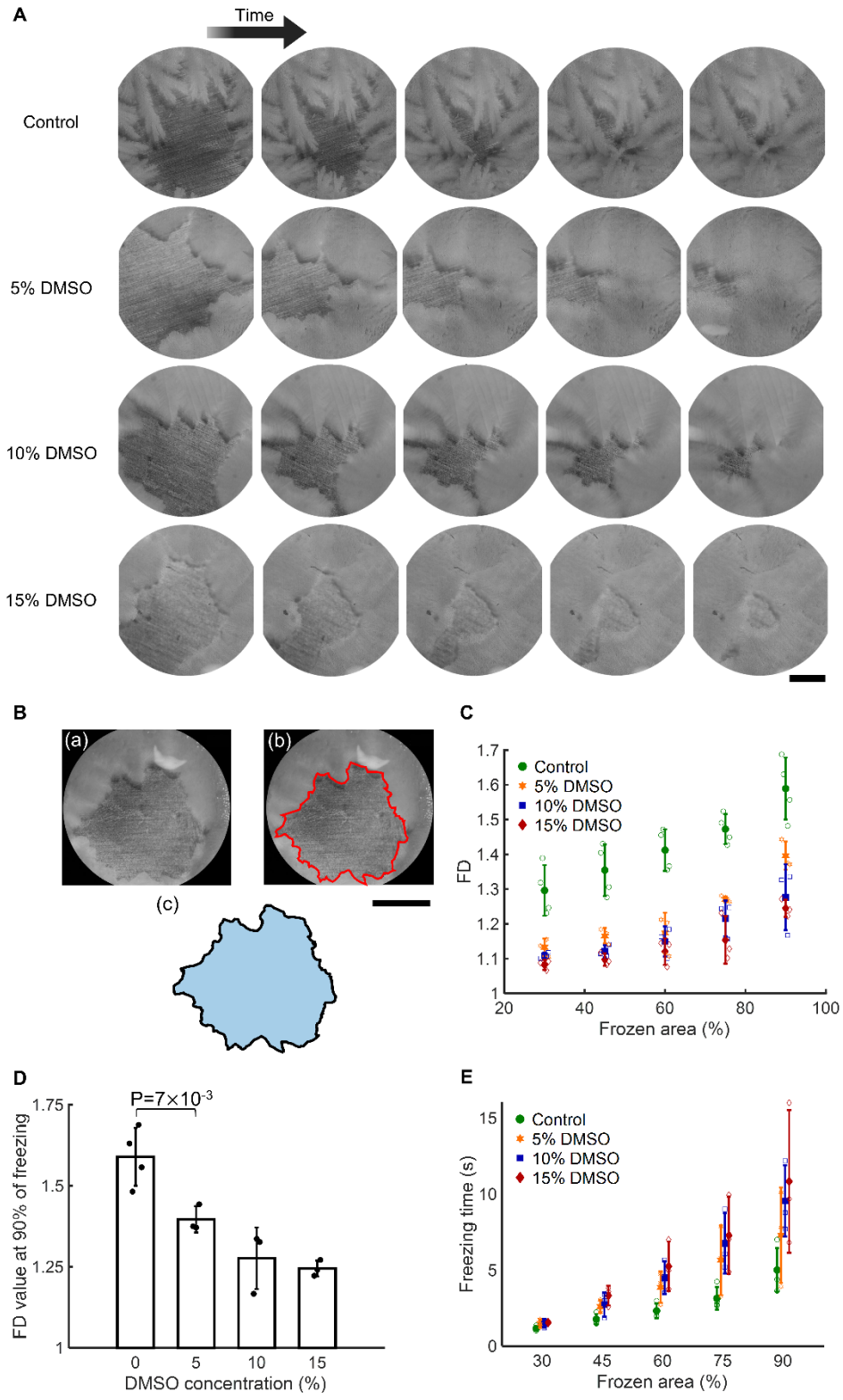

Figure S5.

Ice crystal-formation in the freezing processes of GelMA hydrogel groups with different concentrations of DMSO. (**A**), Representative brightfield time-lapse images of the hydrogel

groups during ice crystal-formation. The shape and the size of the ice crystals were clearly different in the DMSO-free sample. Scale bar: 2 mm. (**B**), Identifying the ice crystals' borderline in a representative image for quantifying the sharpness of the ice crystals. The unfrozen portion of the hydrogel derived as a polygon in panel (c) was used to quantify the ice crystals' sharpness. Scale bar: 2 mm. (**C**), Trend of changes in FD during the hydrogel freezing process. When the sharp crystals formed, the irregularities in the polygon geometry increased, which resulted in a higher FD value. (**D**), FD values for different hydrogels when 90% of the samples in the microscope's field of view became frozen. (**E**), Comparison of the freezing times for different hydrogel bioink groups. The addition of DMSO generally increases the freezing time. t=0 corresponds to when the frozen area is approximately 25% of the microscope's field of view. n = 4.

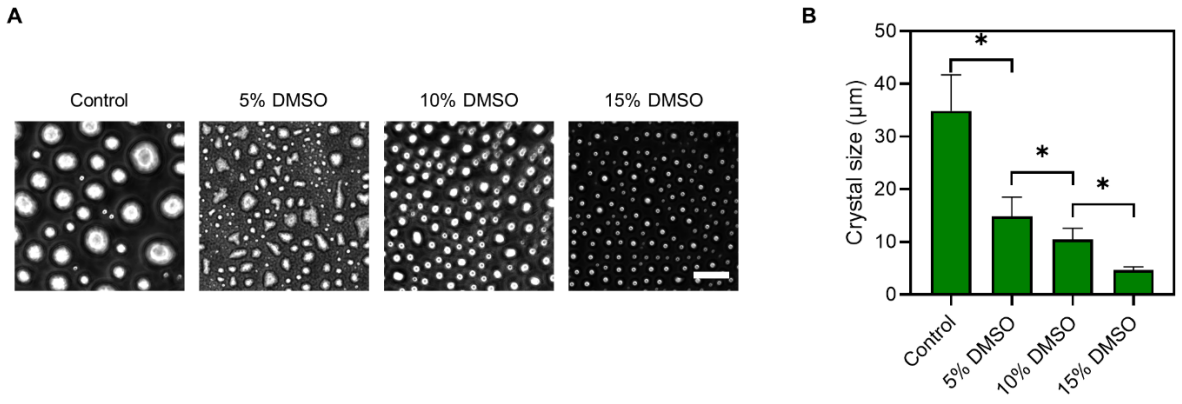

Figure S6.
Effect of DMSO on ice recrystallization-inhibition determined *via* the splat assay. (A), Photographs showing ice crystals grown in GelMA wafers with different concentrations of DMSO. Scale bar: 50 µm. **(B)**, Quantification of the ice crystal size for the study groups. n = 3; *P < 0.05.

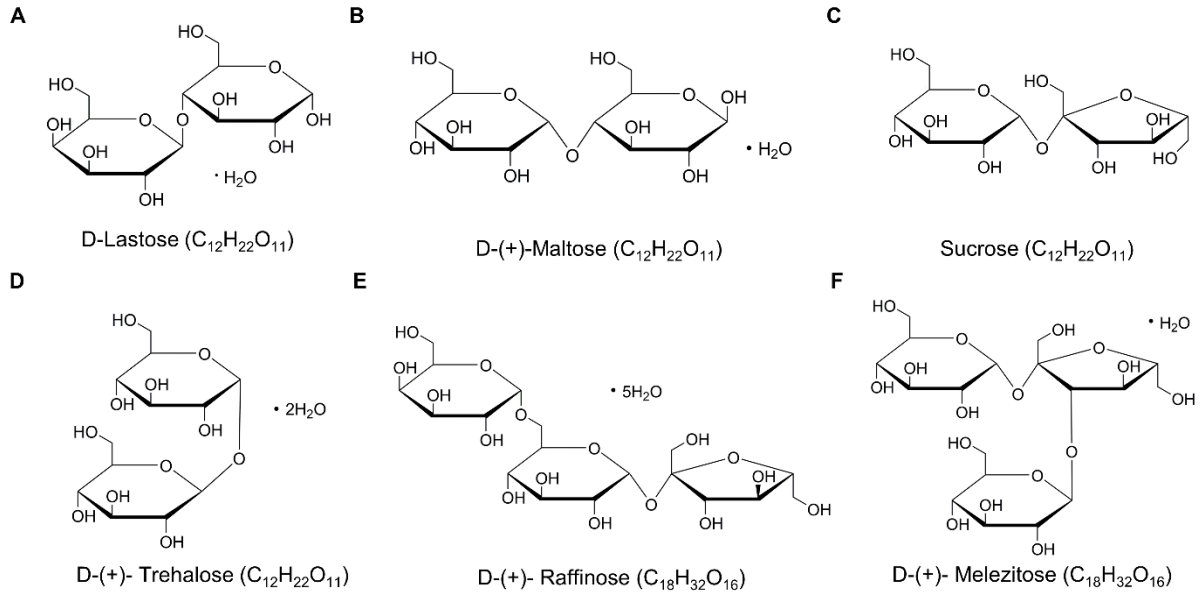

Figure S7.

Chemical structures of the investigated saccharides for cryobioprinting. (**A**), Lactose. (**B**), Maltose. (**C**), Sucrose. (**D**), Trehalose. (**E**), Raffinose. (**F**), Melezitose.

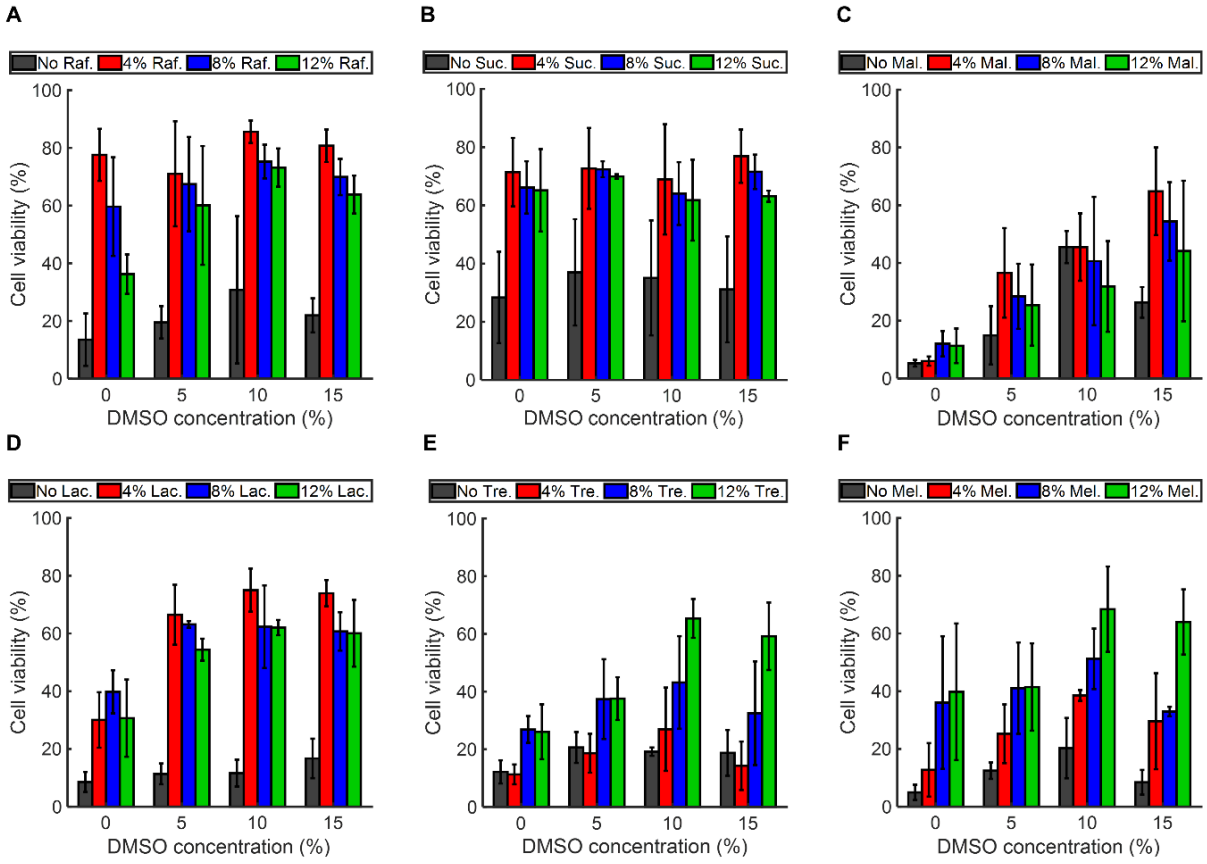

Figure S8.

Cell viability in GelMA hydrogels with different concentrations of DMSO and saccharides cryopreserved for 72 h. (**A**), Raffinose. (**B**), Sucrose. (**C**), Maltose. (**D**), Lactose. (**E**), Trehalose. (**F**), Melezitose. n=3.

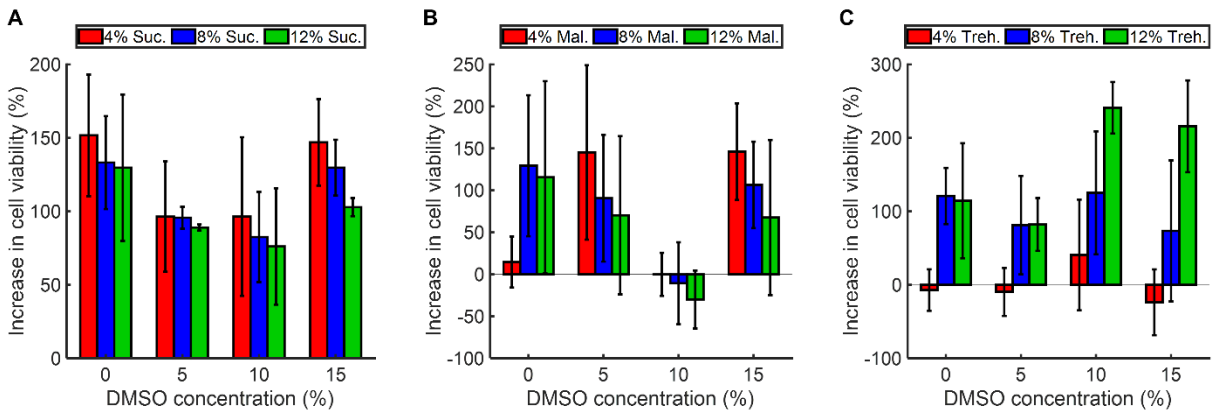

Figure S9.

Quantified increases in cell viability post-cryopreservation for 72 h due to supplementing the cryoprotectant bioink with different saccharides. (**A**), Sucrose. (**B**), Maltose. (**C**), Trehalose. n=3.

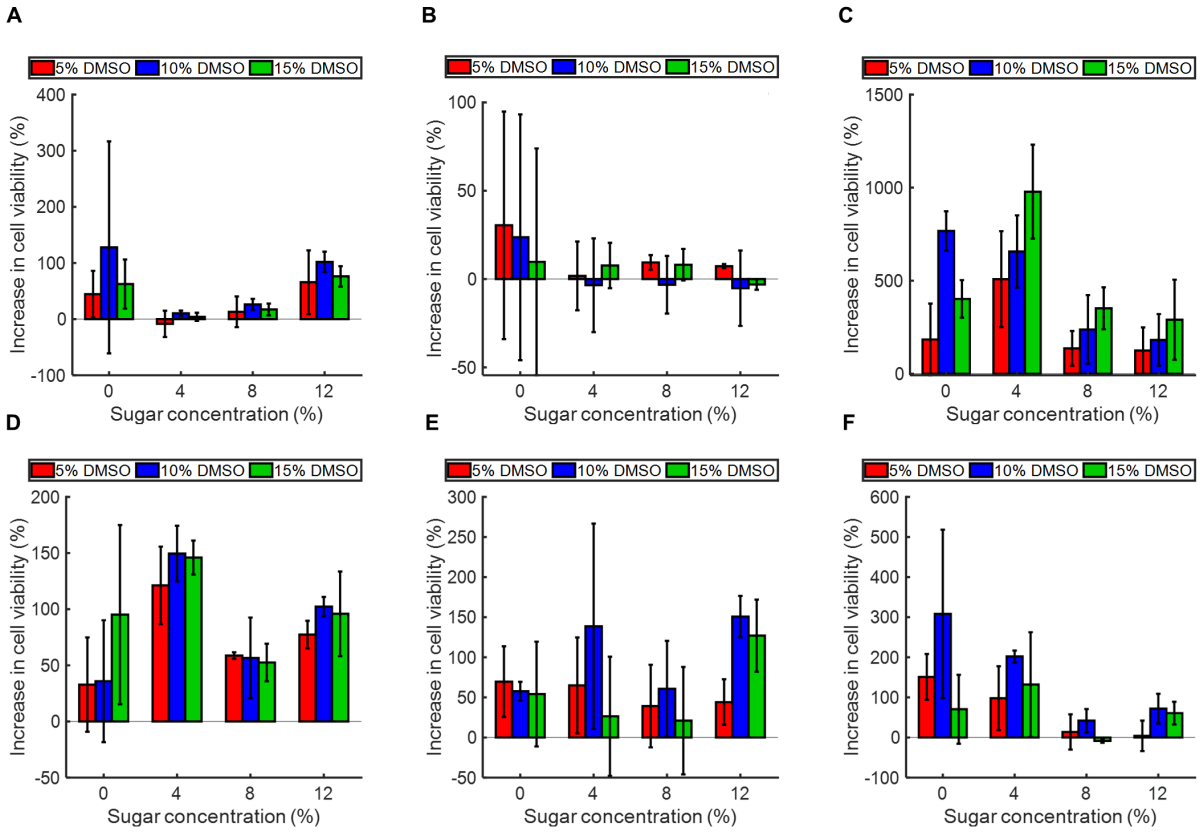

Figure S10.

Quantification of the effect of DMSO in the cryoprotectant bioink formulations on enhancing cell viability post-cryopreservation for 72 h. (**A**), Raffinose. (**B**), Sucrose. (**C**), Maltose. (**D**), Lactose. (**E**), Trehalose. (**F**), Melezitose. n=3.

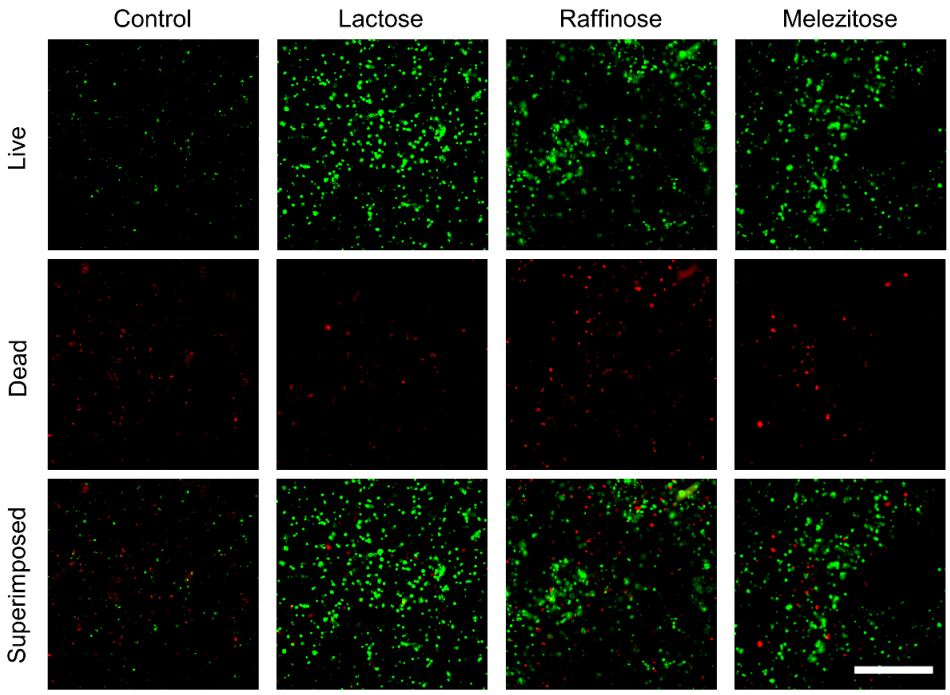

Figure S11.

Representative fluorescence images of the NIH/3T3 fibroblasts encapsulated in the selected cryoprotective bioinks and frozen for 72 h. Scale bar: 500 μm.

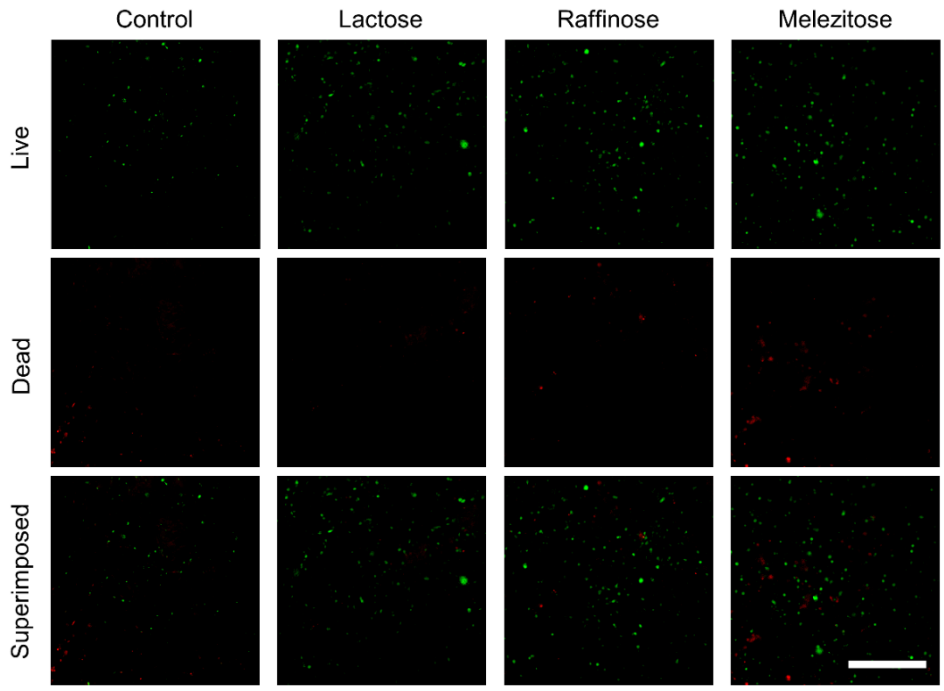

Figure S12.

Representative fluorescence images of the HepG2 cells encapsulated in the selected cryoprotective bioinks and frozen for 72 h. Scale bar: 500 μm.

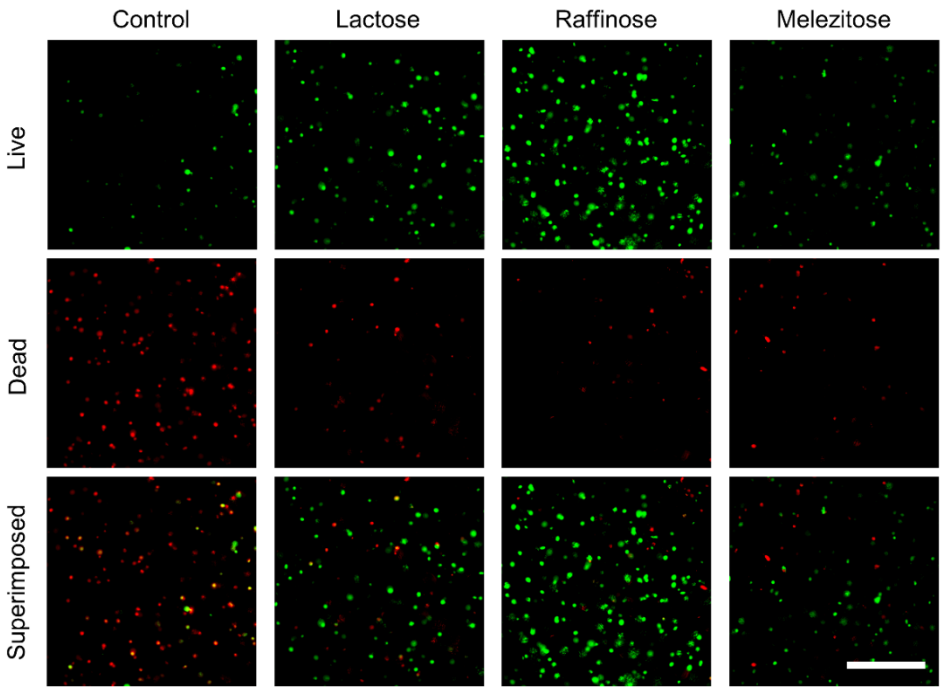

Figure S13.

Representative fluorescence images of the HUVECs encapsulated in the selected cryoprotective bioinks and frozen for 72 h. Scale bar: 500 μm.

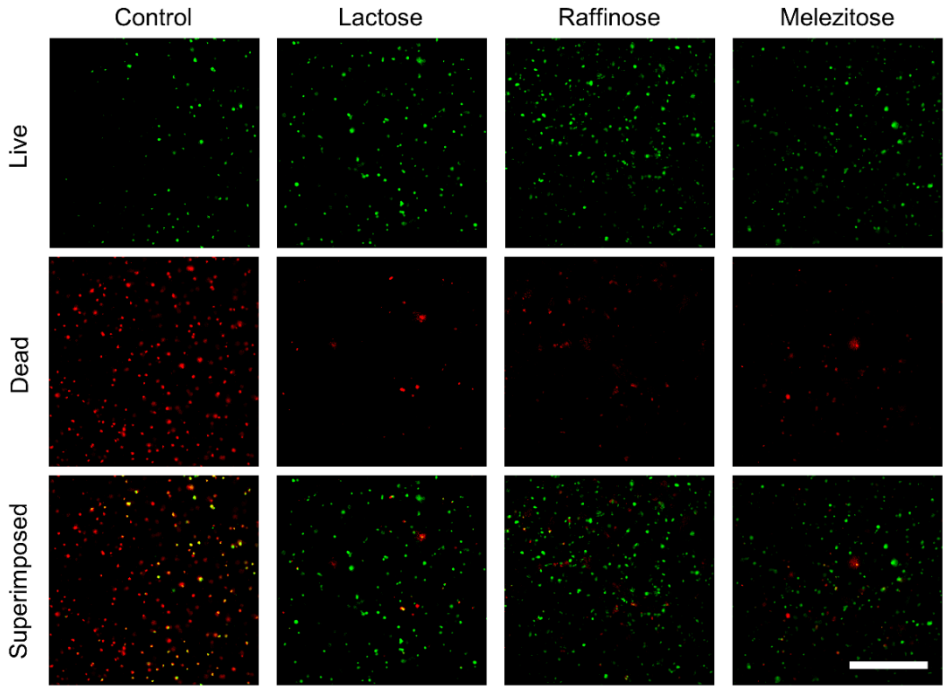

Figure S14.

Representative fluorescence images of the MCF-7 cells encapsulated in the selected cryoprotective bioinks and frozen for 72 h. Scale bar: 500 μm.

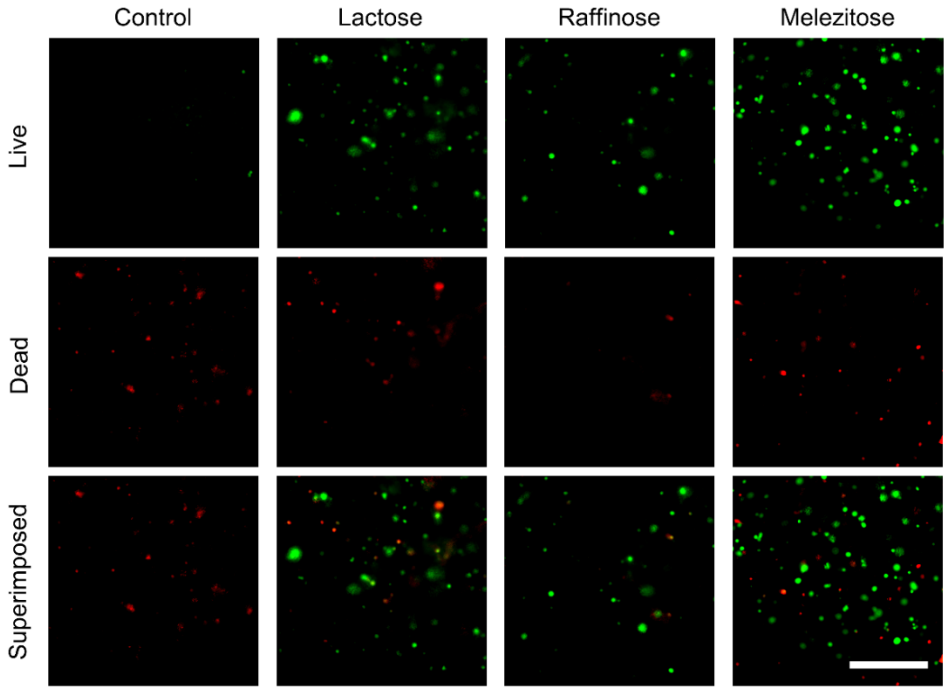

Figure S15.

Representative fluorescence images of the SMCs encapsulated in the selected cryoprotective bioinks and frozen for 72 h. Scale bar: 500 μm.

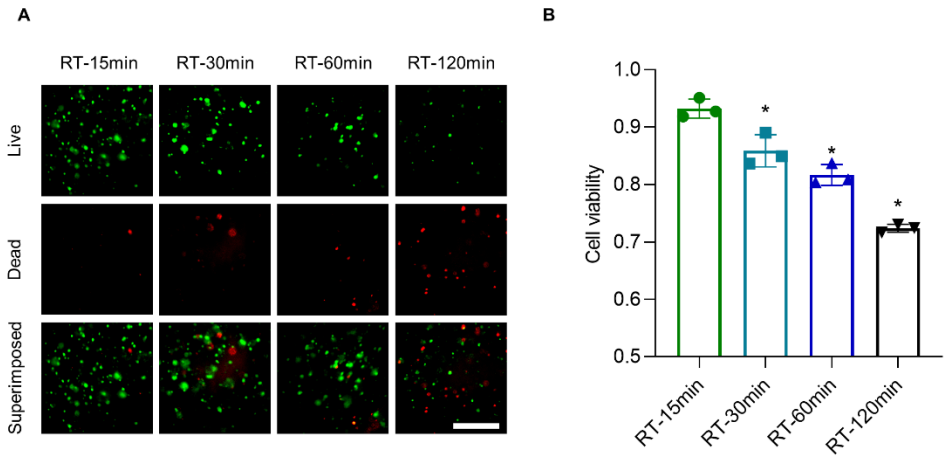

Figure S16.

Effect of keeping NIH/3T3 cells in contact with the selected CPA (DMSO+melezitose) within GelMA for different timespans. (**A**), Fluorescence images. Scale bar: 500 μm. (**B**), Quantification of cell viability. n = 3; *P < 0.05.

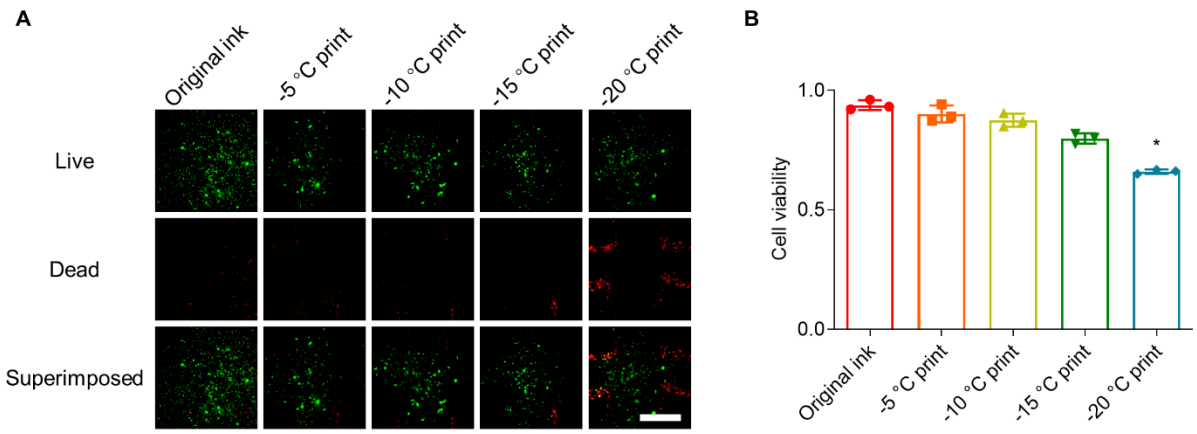

Figure S17.

NIH/3T3 cell viability after cryobioprinting at different temperatures of the freezing plate. (**A**), Fluorescence microscopy images showing viability of cells in the GelMA/CPA matrix. Scale bar: 500 μm. (**B**), Quantification of cell viability. n = 3; *P < 0.05.

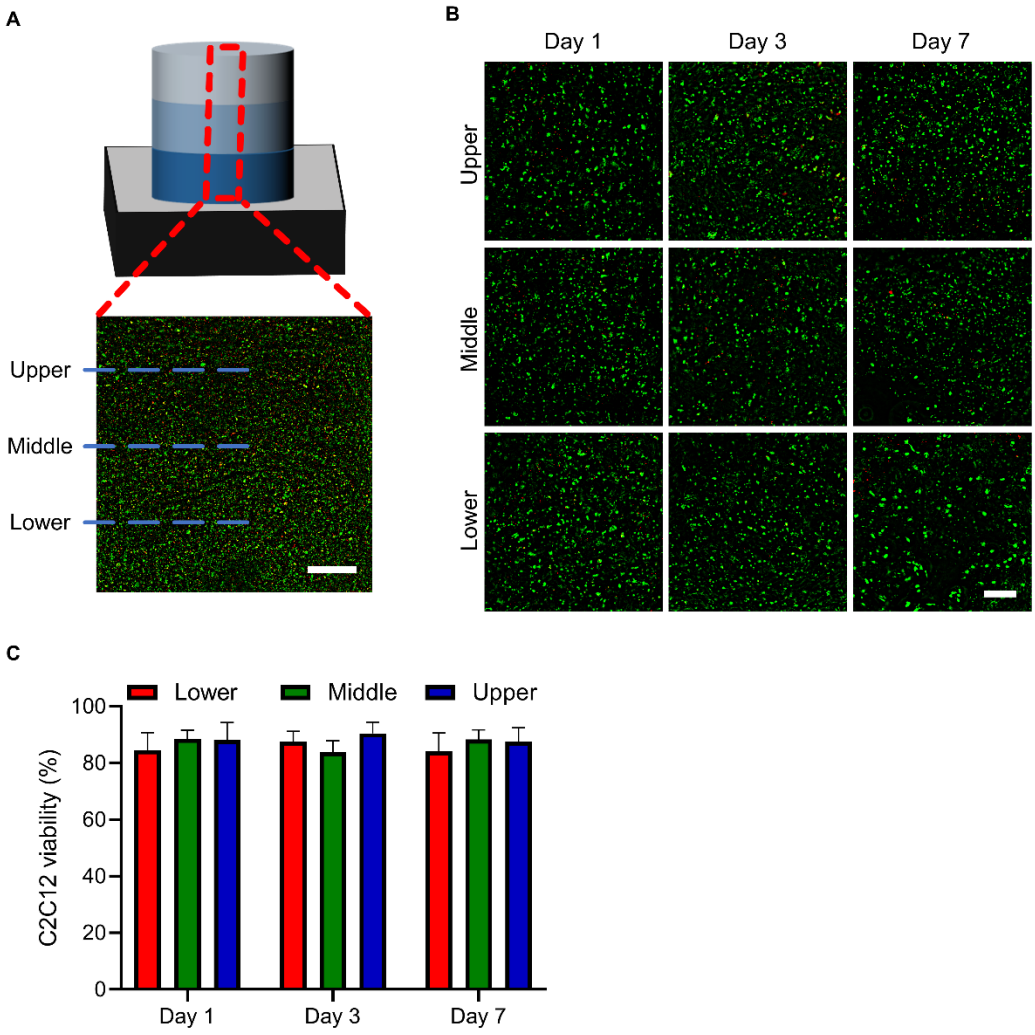

Figure S18.

Cell viability of C2C12 myoblasts in different layers of cryobioprinted cell-laden constructs. (**A**), Schematic and lateral live/dead images of the cryobioprinted scaffold. Scale bar: 2 mm. (**B**), Representative live/dead images of different layers on days 1, 3, and 7. Scale bar: 500 μm. (**C**), Quantification of cell viability in different layers. n=3.

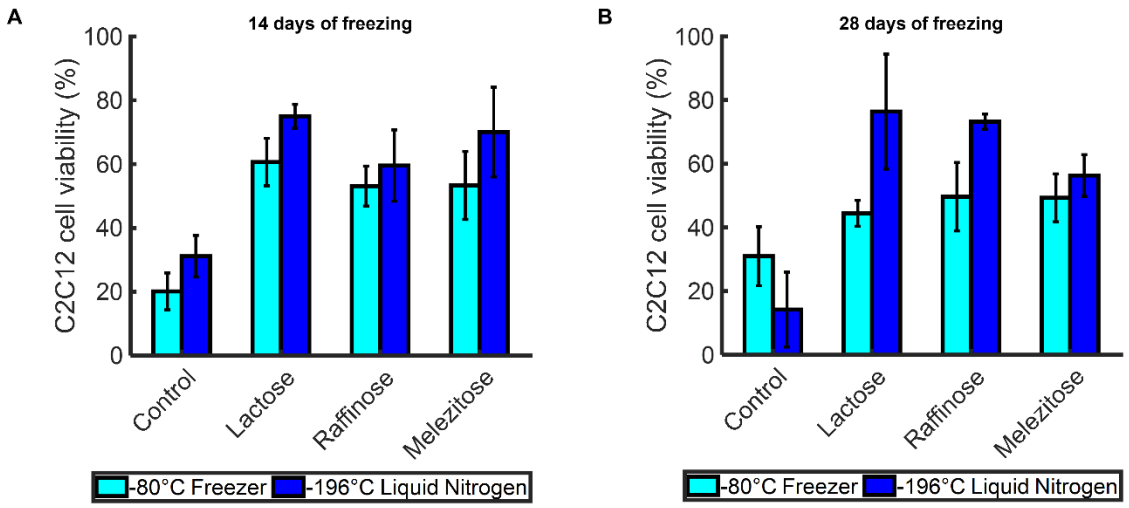

Figure S19.

Effects of cryopreservation on cell viability at -80 °C and -196 °C (liquid nitrogen) in the cryoprotective bioinks with different formulations. (**A**), shorter-term. (**B**), longer-term. n=3.

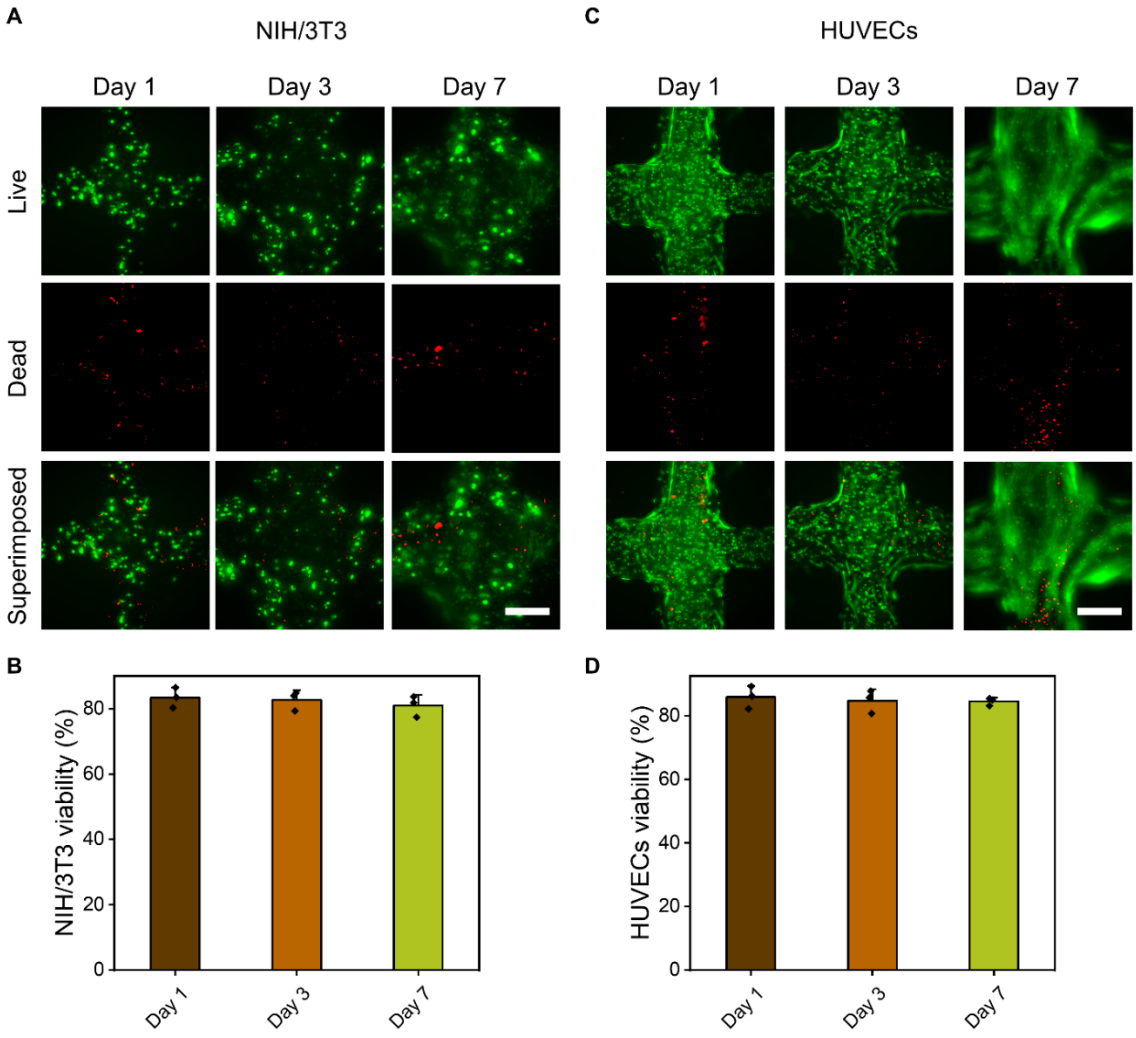

Figure S20.

Cell viability in cryobioprinted cell-laden constructs after 3 months of cryopreservation at -196 °C (liquid nitrogen), at different days post-revival. (**A** and **B**), NIH/3T3. (**C** and **D**), HUVECs. Scale bars: 500 μm.

Table S1.

Temperature control of the freezing plate at room temperature.

Voltage (V)	Current (A)	Environment temperature (ºC)	Cooling water temperature (ºC)	Freezing plate temperature (ºC)
0	0	23.0	1.0	11.0
2.00	0.47	23.0	1.0	-4.5
4.00	0.96	23.0	1.0	-12.2
6.00	1.48	23.0	1.0	-17.5
8.00	1.98	23.0	1.0	-22.3
10.00	2.49	23.0	1.0	-25.0
12.00	3.01	23.0	1.0	-27.2

Table S2.

Temperature control of the freezing plate in the cold room.

Voltage (V)	Current (A)	Environment temperature (ºC)	Cooling water temperature (ºC)	Freezing plate temperature (ºC)
0	0	5.0	1.0	4.0
2.00	0.47	5.0	1.0	-6.0
4.00	0.97	5.0	1.0	-12.7
6.00	1.49	5.0	1.0	-19.2
8.00	2.03	5.0	1.0	-24.9
10.00	2.55	5.0	1.0	-27.8
12.00	3.04	5.0	1.0	-29.5

Table S3.

Freezing rates in the first two layers for different values of T_p. The values are derived from the heat-transfer simulation.

		T_p (°C)			
		5	**10**	**15**	**20**
Freezing rate (°C s^{-1})	**1st layer**	43.89	62.89	81.33	100.00
	2nd layer	2.69	3.28	4.35	5.60

Table S4.
Heat-transfer simulation parameters.

Parameter	Value
Thermal conductivity (W m^{-1} K^{-1})	0.57
Density (kg m^{-3})	1,000
Heat capacity (J kg^{-1} K^{-1})	4,136
Ratio of specific heats	1.33
Bioink's initial temperature (°C)	15
Ambient temperature (°C)	20